Supplement of The Cryosphere, 20, 4911–4925, 2026
https://doi.org/10.5194/tc-20-4911-2026-supplement

Supplement of

Predictability of summertime diurnal winds over ungauged mountain glaciers

Jayan Krishnanand et al.

Correspondence to: Argha Banerjee (argha@iiserpune.ac.in)

S1. Relationship between Eq. 1 and linear response

We define the Fourier transform of a time-domain function $f(t)$ as:

$$\hat{f}(\omega) = \int_{-\infty}^{\infty} f(t)e^{i\omega t}dt. \tag{S1}$$

The linear-response model, which assumes that the variation in glacier wind speed is a linear response to the diurnal variation of temperature, is given by:

$$u_d + \tau_0 \frac{d}{dt}u_d = sT_d. \tag{S2}$$

While the present empirical model (Eq. 1) assumes the following relation:

$$u_d + s\tau \frac{d}{dt}T_d = sT_d. \tag{S3}$$

The symbols s_0 and τ_0 above denote the sensitivity of the wind to temperature forcing and the response time, respectively, for the linear-response model. Note that these two parameters are in general different from the corresponding sensitivity s and response time τ in the empirical model, in general. Taking Fourier transform on both sides of this equation (Eq. S2), we obtain:

$$(1 - i\omega\tau_0)\hat{u}_d = s_0\hat{T}_d \tag{S4}$$

$$\implies \hat{u}_d = \frac{s_0}{(1 - i\omega\tau_0)}\hat{T}_d. \tag{S5}$$

$$\implies \hat{u}_d = \frac{s_0}{(1 + \omega^2\tau_0^2)}(1 + i\omega\tau_0)\hat{T}_d. \tag{S6}$$

In the limit of $\omega^2\tau_0^2 << 1$, this form is similar to the one obtained by taking Fourier transform on both sides of equation S3):

$$\hat{u}_d = s(1 + i\omega\tau)\hat{T}_d. \tag{S7}$$

For the mean hourly summer temperature and wind speed considered here, the dominant frequency is $\omega = 2\pi/24$ hours. Given that the response time $\tau \approx 1$ hr, we are in this low-frequency limit. Thus, for the problem of mean diurnal variability of wind speed addressed here, our empirical model (Equation S4) is equivalent to the linear response model (Eq. S3).

S2. Top three predictors for $\bar{u}, s$ and τ

As discussed in Sect. 4.1.2, the three best performing predictors for $\bar{u}$ and their R^2 values are shown below:

$$\bar{u} = (0.268 \pm 0.017)\sqrt{\frac{|\bar{T}|}{\varsigma_{10}}}, \qquad R^2 = 0.90\,(p < 0.001), \tag{S8}$$

$$\bar{u} = (0.45 \pm 0.04)\sqrt{\frac{|\bar{T}|}{\varsigma_g}}, \qquad R^2 = 0.83\,(p > 0.01), \tag{S9}$$

$$\bar{u} = (0.97 \pm 0.09)\sqrt{\frac{|\bar{T}|}{Z_{range}/W_g}}, \qquad R^2 = 0.79\,(p > 0.01), \tag{S10}$$

where $|\bar{T}|$ is the absolute value of mean summertime temperature, ς_g is the slope of 10-km topography ς_g is the mean glacier slope, Z_{range} is the elevation range of the glacier, and W_g is the mean glacier width (Table S2). The value of $\bar{u}$ predicted by Eq. S8 have been plotted against its best-fit values in S3.

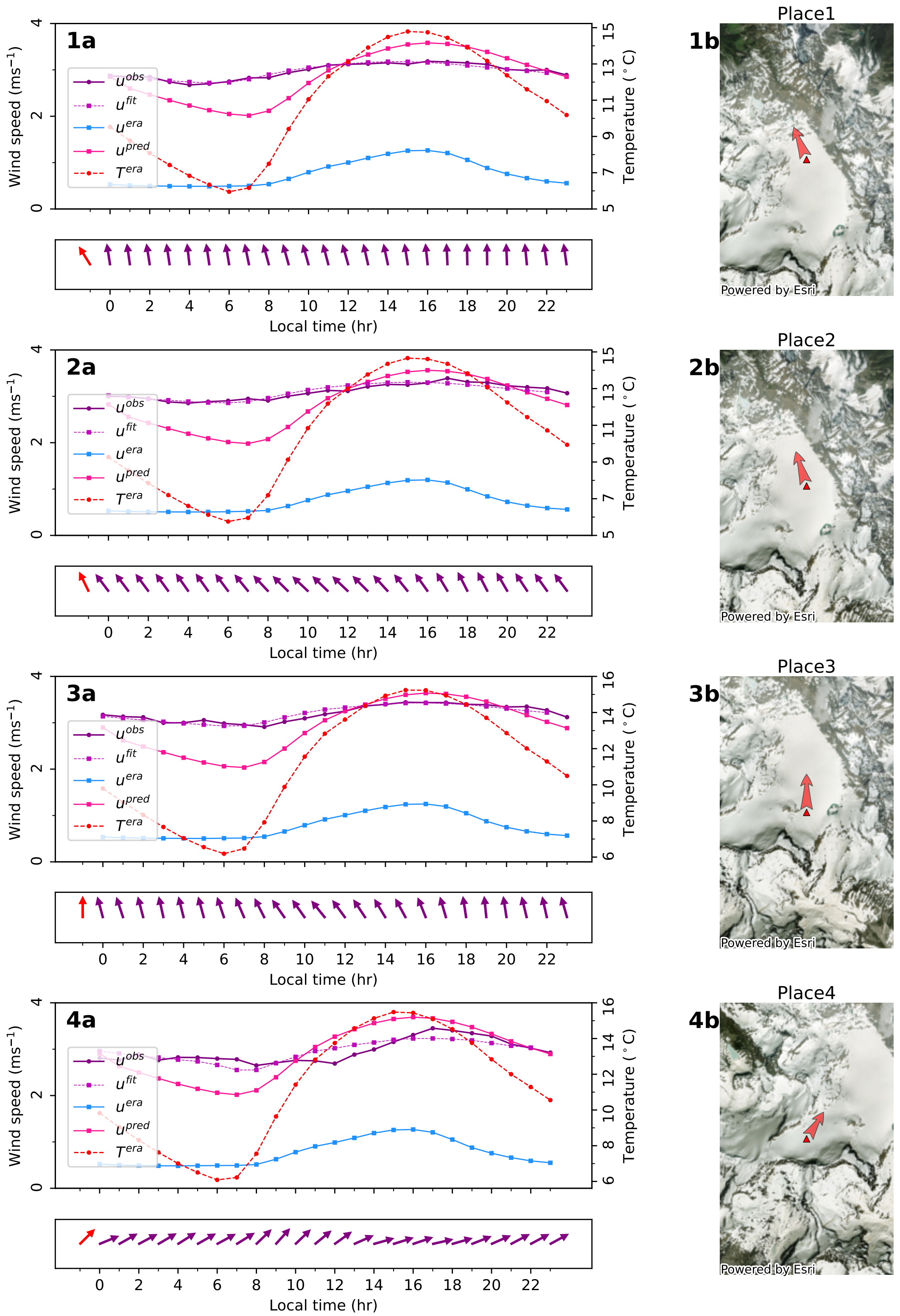
1a
2a
3a
4a
u^{obs}
u^{fit}
u^{era}
u^{pred}
T^{era}
Wind speed (ms^{-1})
Temperature (°C)
Local time (hr)
1b
2b
3b
4b
Place1
Place2
Place3
Place4
Powered by Esri

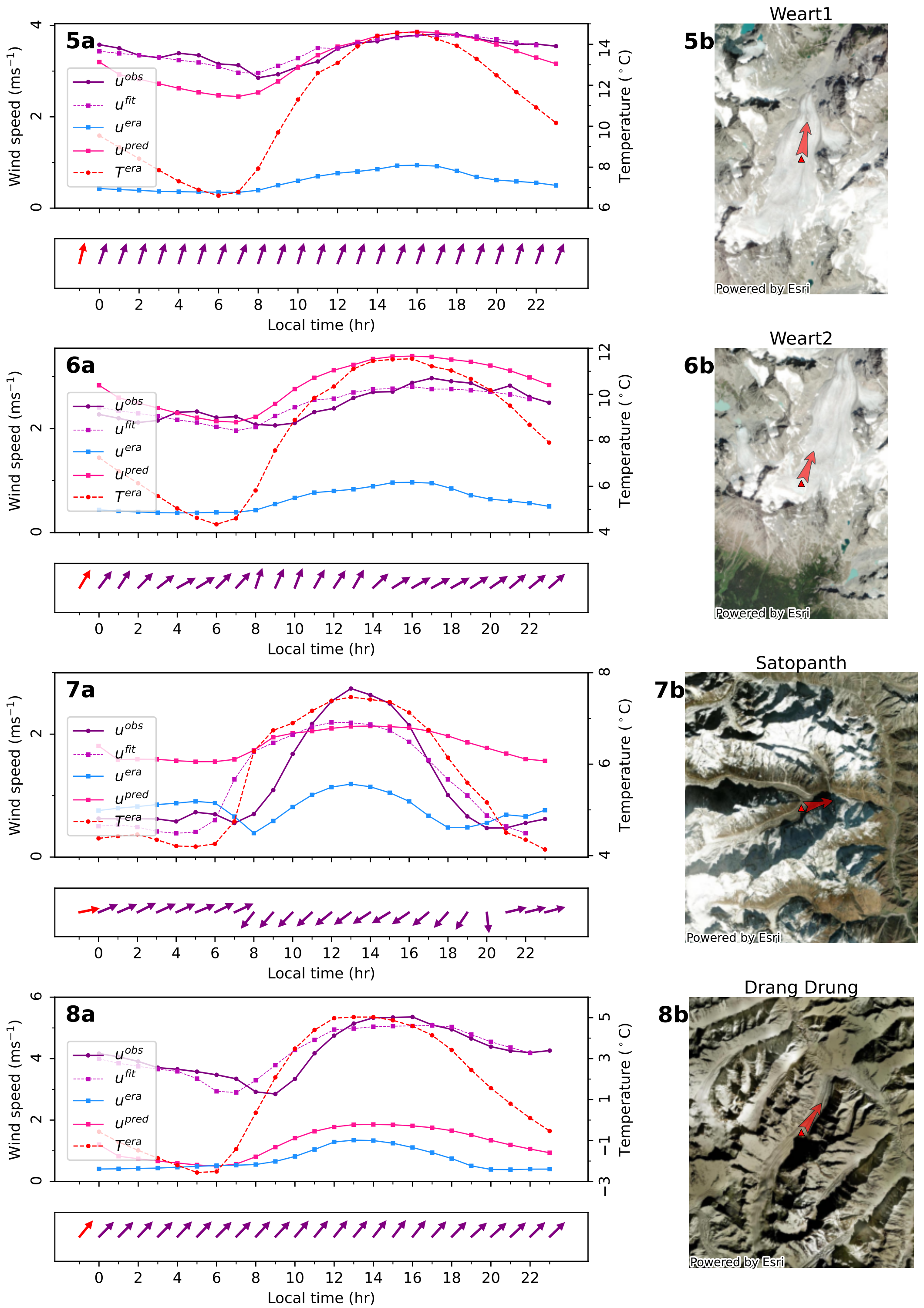
5a
6a
7a
8a
5b
6b
7b
8b
Weart1
Weart2
Satopanth
Drang Drung
Wind speed (ms^{-1})
Temperature ($^\circ$C)
Local time (hr)
u^{obs}
u^{fit}
u^{era}
u^{pred}
T^{era}
Powered by Esri

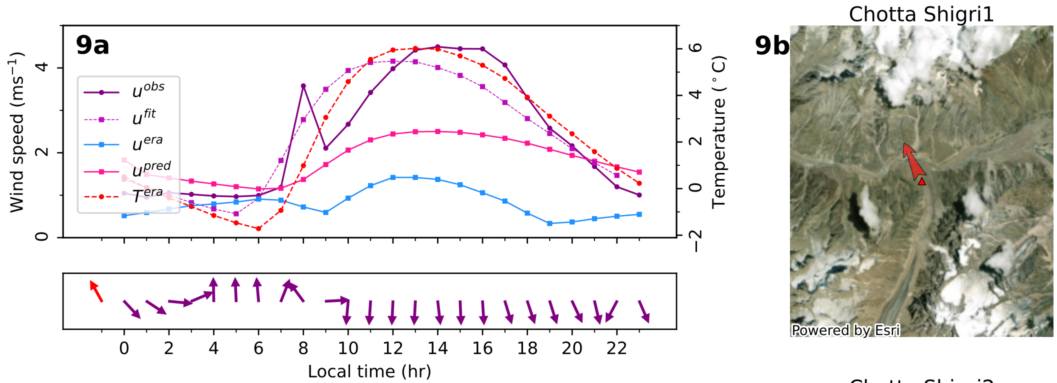
9a
Wind speed (ms−1)
Temperature (°C)
u^obs
u^fit
u^era
u^pred
T^era
Local time (hr)
9b
Chotta Shigri1
Powered by Esri

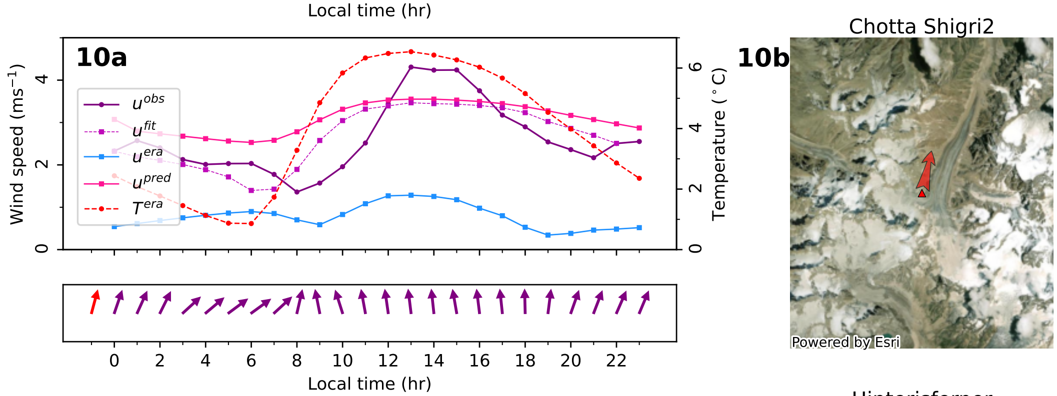
10a
Wind speed (ms−1)
Temperature (°C)
u^obs
u^fit
u^era
u^pred
T^era
Local time (hr)
10b
Chotta Shigri2
Powered by Esri

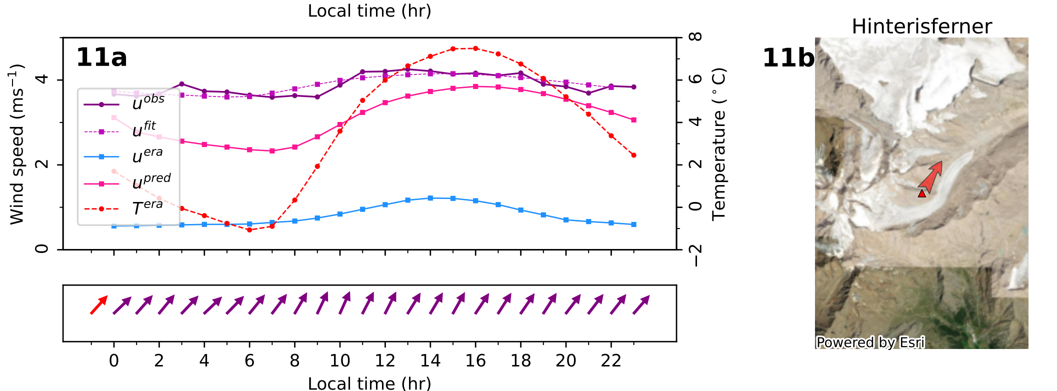
11a
Wind speed (ms−1)
Temperature (°C)
u^obs
u^fit
u^era
u^pred
T^era
Local time (hr)
11b
Hinterisferner
Powered by Esri

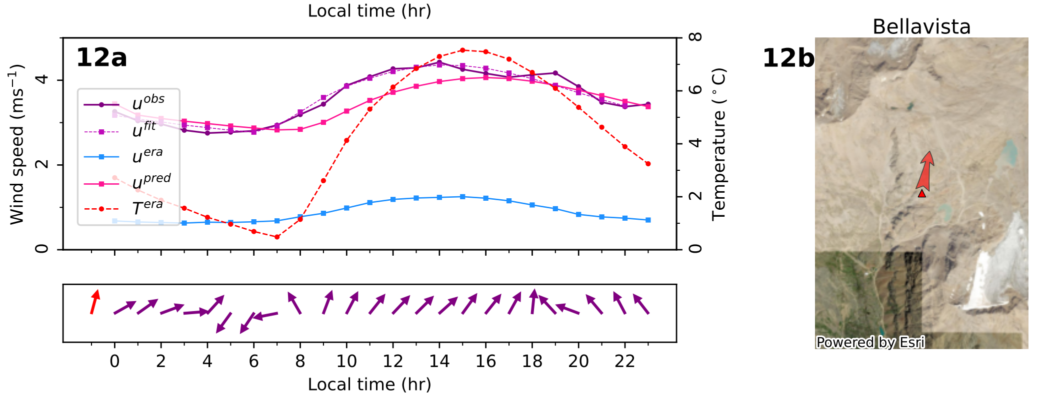
12a
Wind speed (ms−1)
Temperature (°C)
u^obs
u^fit
u^era
u^pred
T^era
Local time (hr)
12b
Bellavista
Powered by Esri

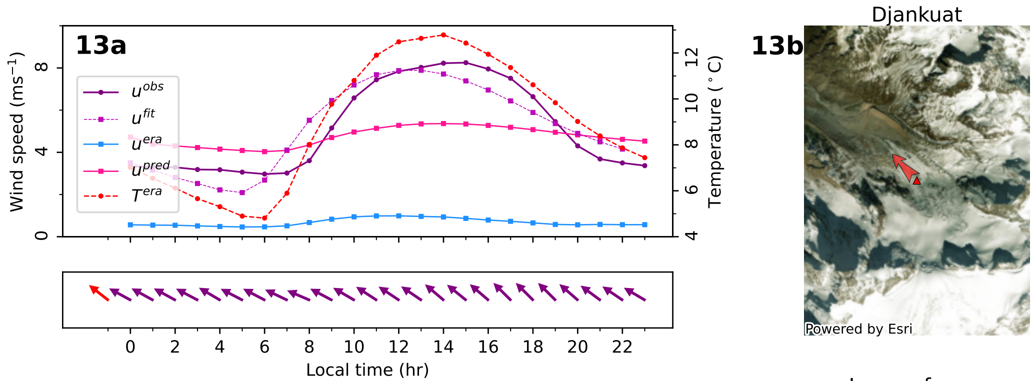
13a
13b
Djankuat
Wind speed (ms^{-1})
Temperature ($^\circ$C)
u^{obs}
u^{fit}
u^{era}
u^{pred}
T^{era}
Local time (hr)
Powered by Esri

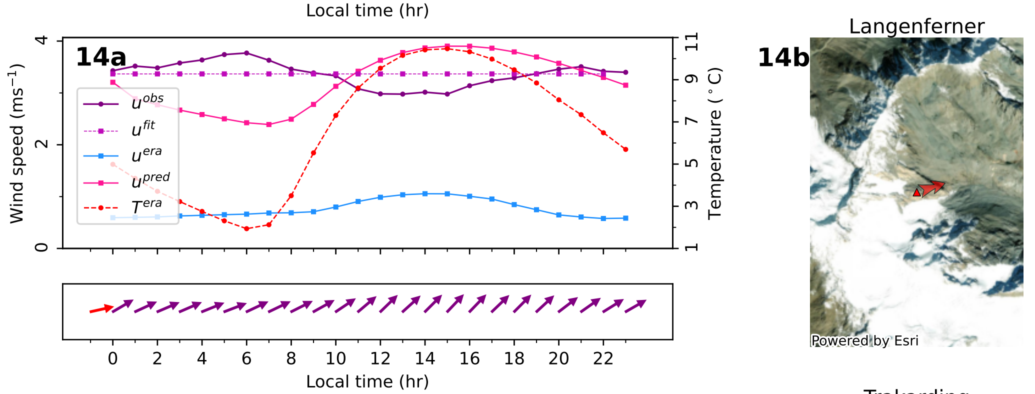
14a
14b
Langenferner
Wind speed (ms^{-1})
Temperature ($^\circ$C)
u^{obs}
u^{fit}
u^{era}
u^{pred}
T^{era}
Local time (hr)
Powered by Esri

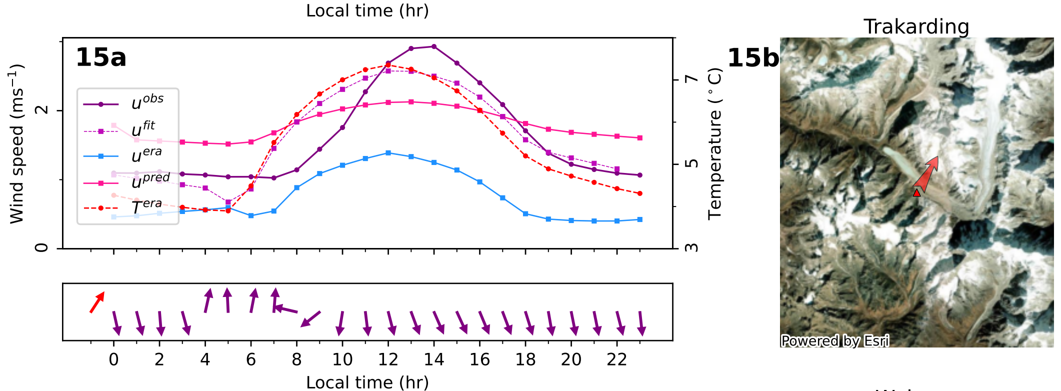
15a
15b
Trakarding
Wind speed (ms^{-1})
Temperature ($^\circ$C)
u^{obs}
u^{fit}
u^{era}
u^{pred}
T^{era}
Local time (hr)
Powered by Esri

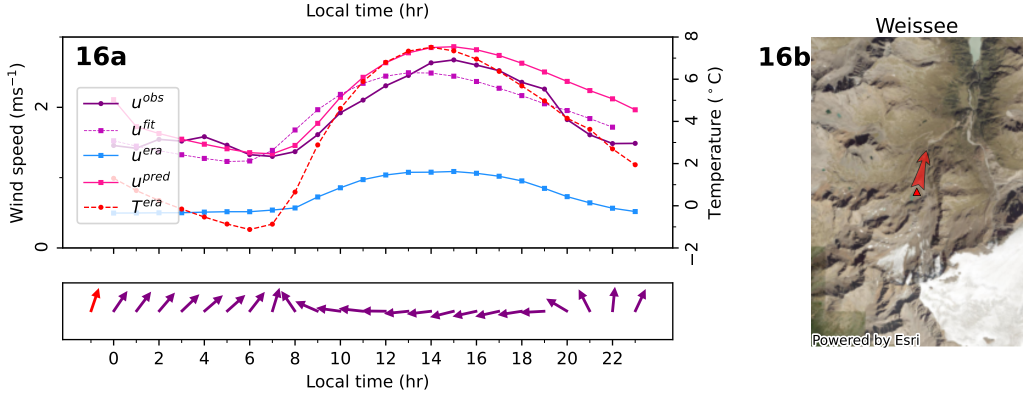
16a
16b
Weissee
Wind speed (ms^{-1})
Temperature ($^\circ$C)
u^{obs}
u^{fit}
u^{era}
u^{pred}
T^{era}
Local time (hr)
Powered by Esri

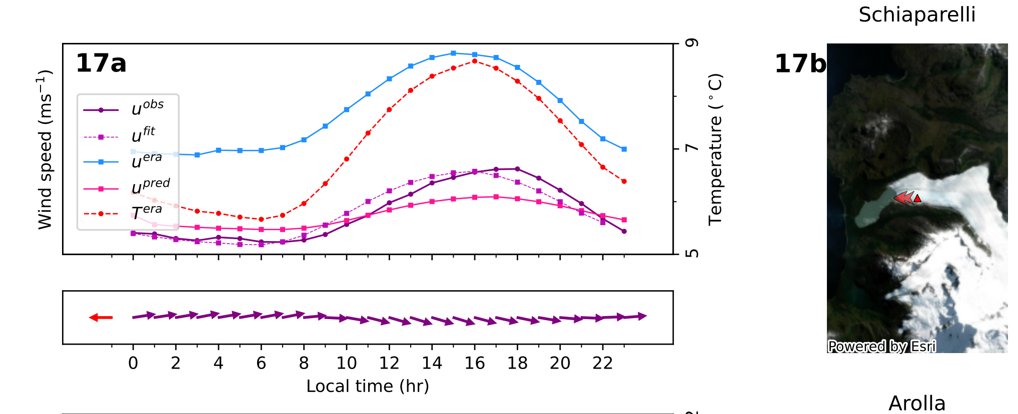
Schiaparelli
17a
17b
Wind speed (ms−1)
Temperature (°C)
Local time (hr)
Powered by Esri

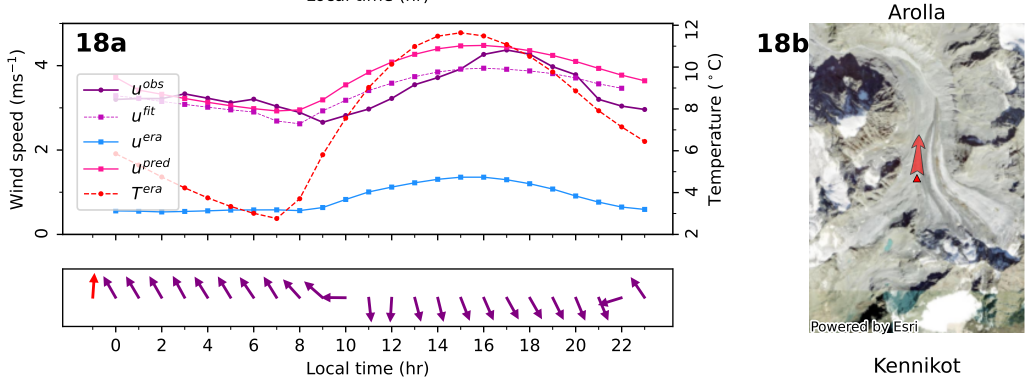
Arolla
18a
18b
Wind speed (ms−1)
Temperature (°C)
Local time (hr)
Powered by Esri

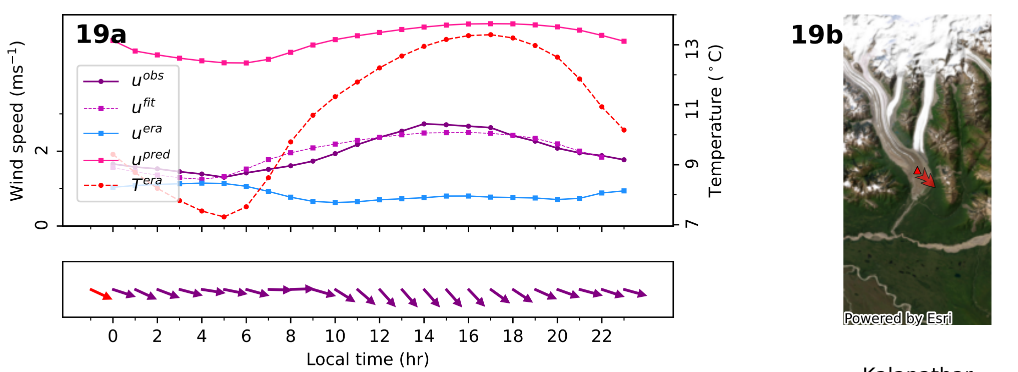
Kennikot
19a
19b
Wind speed (ms−1)
Temperature (°C)
Local time (hr)
Powered by Esri

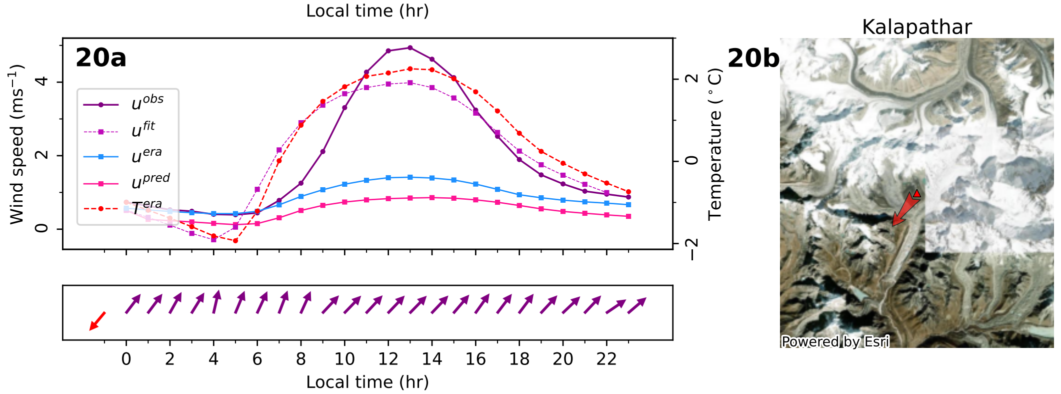
Kalapathar
20a
20b
Wind speed (ms−1)
Temperature (°C)
Local time (hr)
Powered by Esri

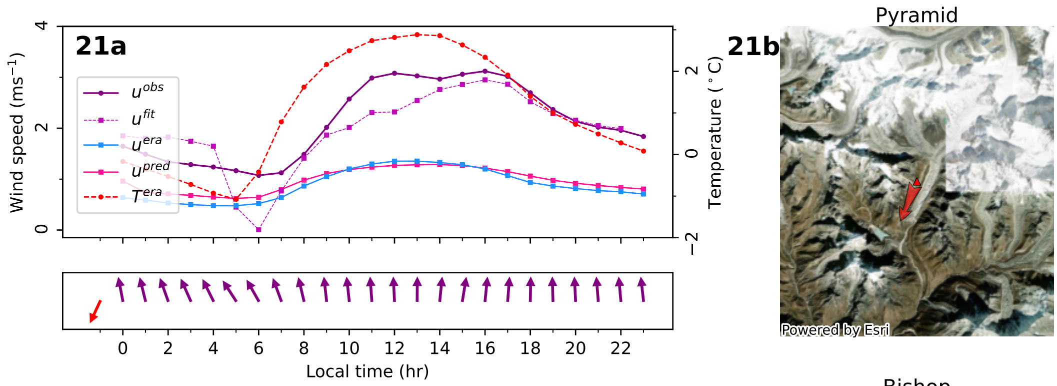
21a
Wind speed (ms^{-1})
Temperature ($^\circ$C)
u^{obs}
u^{fit}
u^{era}
u^{pred}
T^{era}
Local time (hr)
21b
Pyramid
Powered by Esri

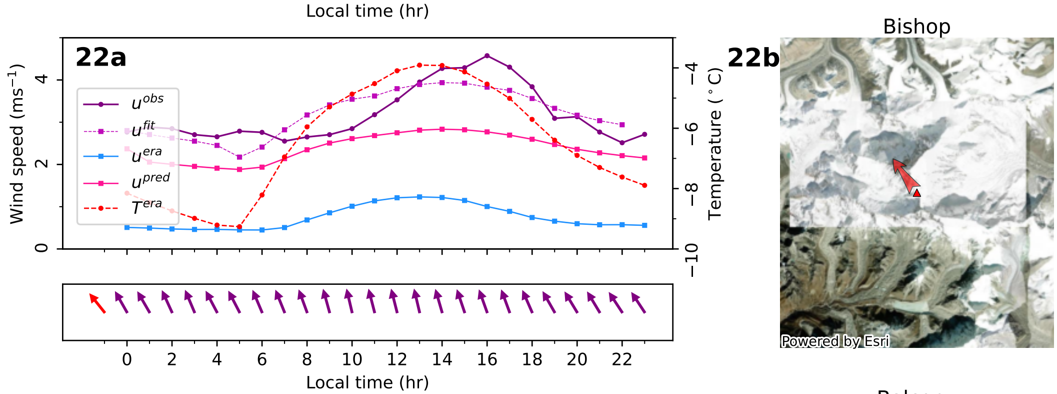
22a
Wind speed (ms^{-1})
Temperature ($^\circ$C)
u^{obs}
u^{fit}
u^{era}
u^{pred}
T^{era}
Local time (hr)
22b
Bishop
Powered by Esri

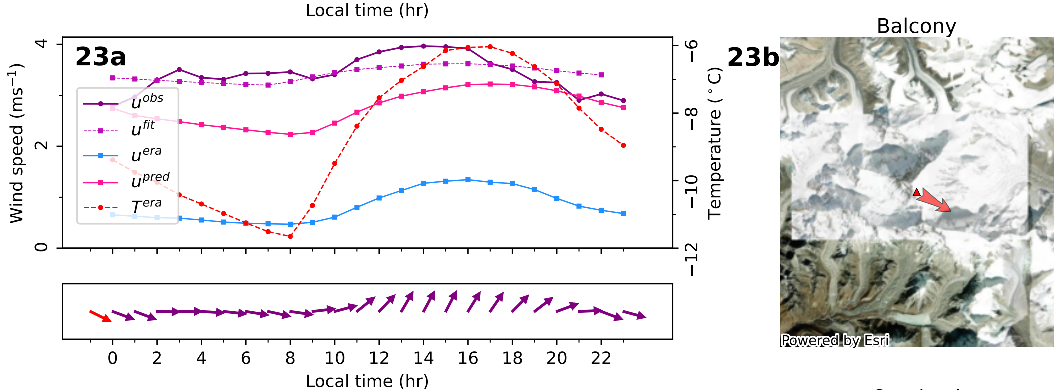
23a
Wind speed (ms^{-1})
Temperature ($^\circ$C)
u^{obs}
u^{fit}
u^{era}
u^{pred}
T^{era}
Local time (hr)
23b
Balcony
Powered by Esri

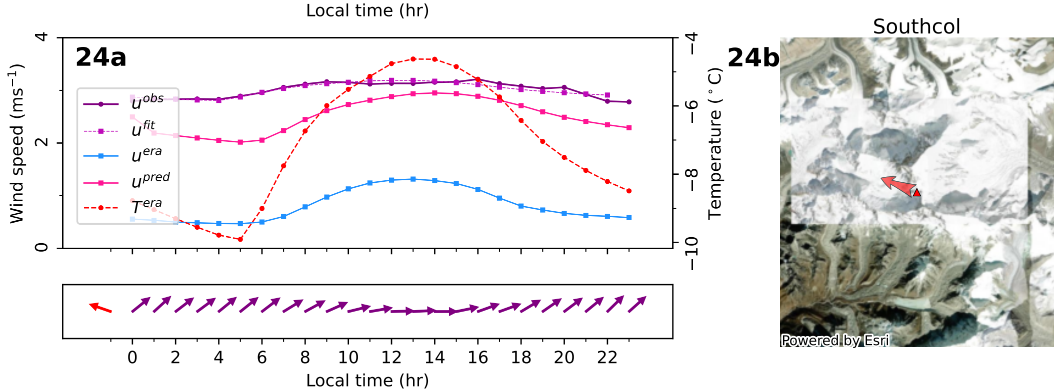
24a
Wind speed (ms^{-1})
Temperature ($^\circ$C)
u^{obs}
u^{fit}
u^{era}
u^{pred}
T^{era}
Local time (hr)
24b
Southcol
Powered by Esri

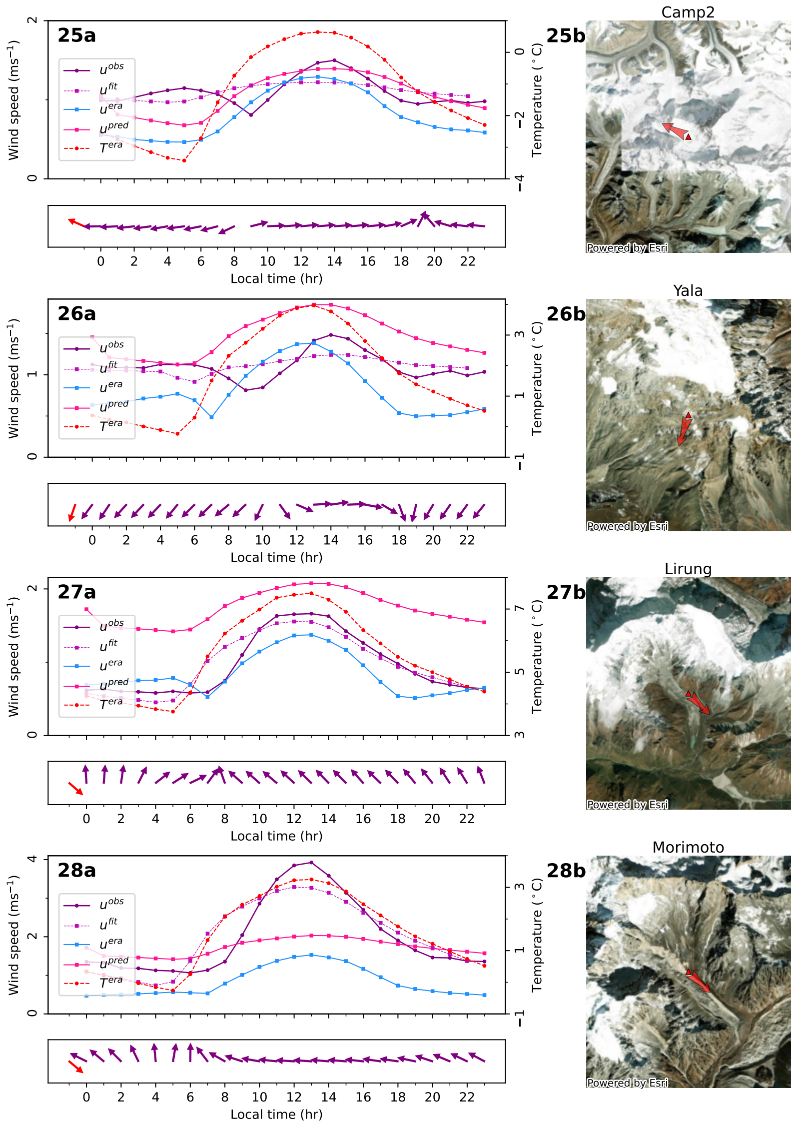

Figure S1. Comparison of model predictions with observations for each of the 28 stations. a) Here u^{obs} denotes the mean hourly values of observed wind speed, u^{fit} denotes the result of fitting Eq. 1 to observations, T^{era} is the ERA5L temperature, u_{pred} denotes the wind speeds predicted using Eqs. 1, 7–9, and ERA5L derived 10m-winds are shown as u^{era}. The purple arrows in the panel below denote the hourly averaged wind vectors for the station, with wind blowing to the north being denoted by an upward arrow. Arrow lengths were rescaled separately for each station so that variations across hours are visible; thus, their lengths are not comparable between stations. The red arrow denotes down-glacier direction which was determined visually from Google Earth. b) The location of weather station (red triangle) on an image of the glacier. The red arrow denotes the down valley direction, which was determined manually. Image Source: Esri, i-cubed, USDA, USGS, AEX, GeoEye, Getmapping, Aerogrid, IGN, IGP, UPR-EGP, and the GIS User Community | Powered by Esri.

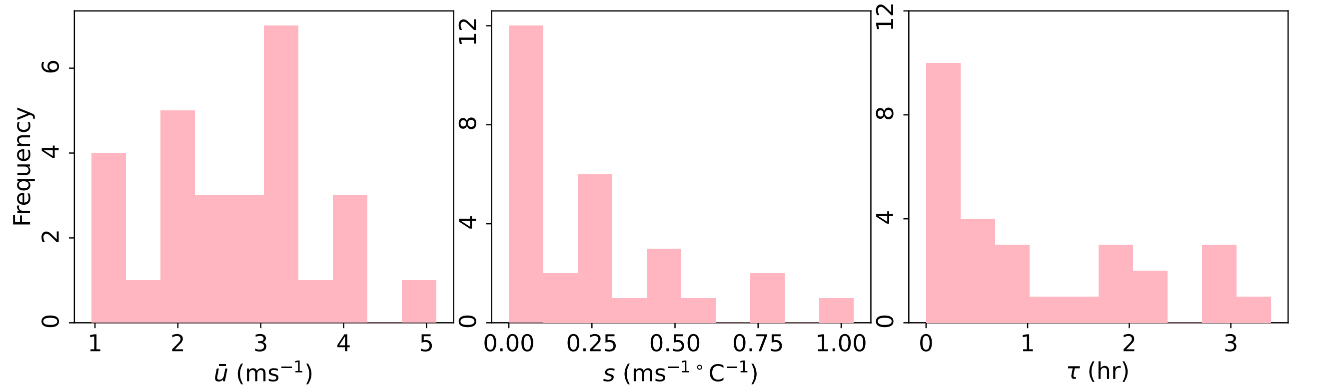

Figure S2. Distribution of model parameters mean wind speed $\overline{u}$, sensitivity of wind speed variation to temperature s and response time τ obtained through fitting Eq. 1 to observations in all 28 stations (main text, section 3.2.1).

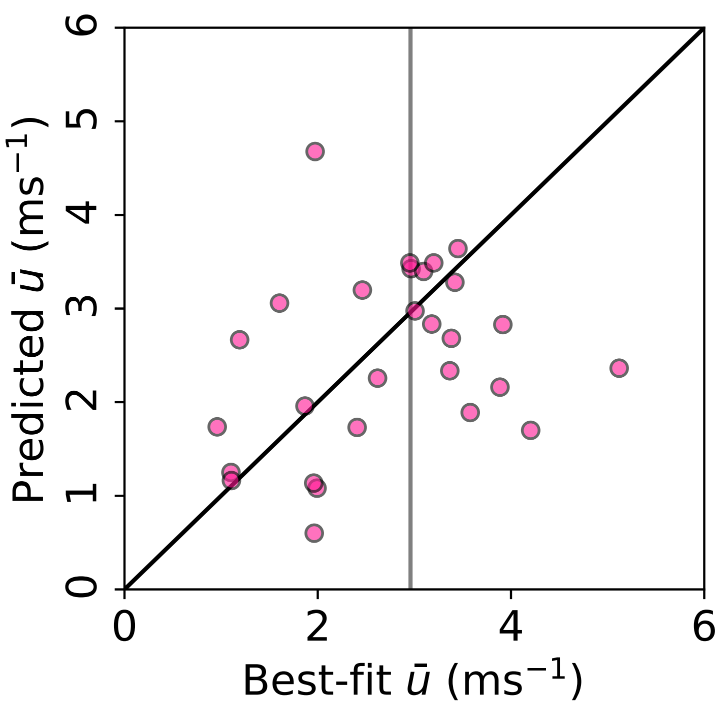

Figure S3. The predictor $\sqrt{|\bar{T}|/\varsigma_g}$, was found to be the second best predictor of mean wind parameter $\bar{u}$. The R^2 value of this predictor was 0.83, but was not significant in $p < 0.01$ limit.

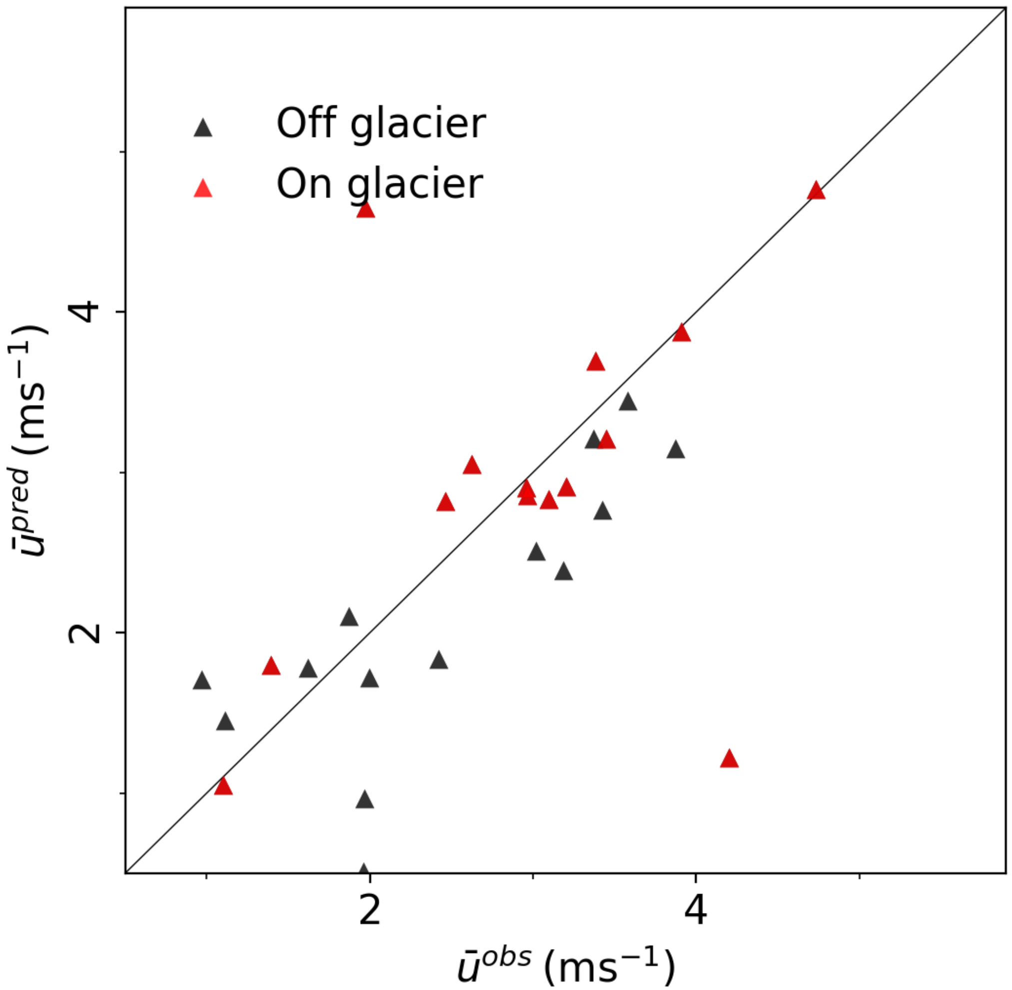

Figure S4. Prediction of mean wind speed versus their best-fit values across 28 stations are shown as red and black triangles. The model prediction for on-glacier stations are coloured red, and that for off-glacier stations is coloured black. The performance of the model was similar for both the subsets of stations.

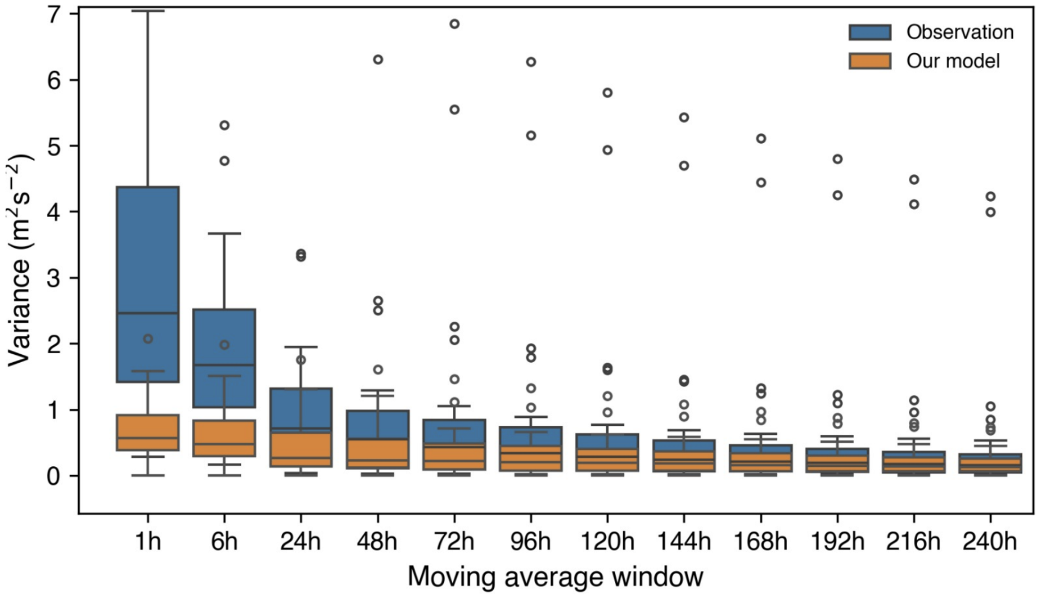

Figure S5. The variance of observed and predicted wind speeds for different time averaging windows from 1 hour to 240 hours across the 28 stations. While the variance of the observed wind speeds came down as the time averaging length increased, variance of predicted winds remain more or less constant across all time-averaging windows. This illustrates that the improvement in wind speed prediction by our model at shorter time-scales (Sect. 5.2.1) is not simply due to a reduction in variance.

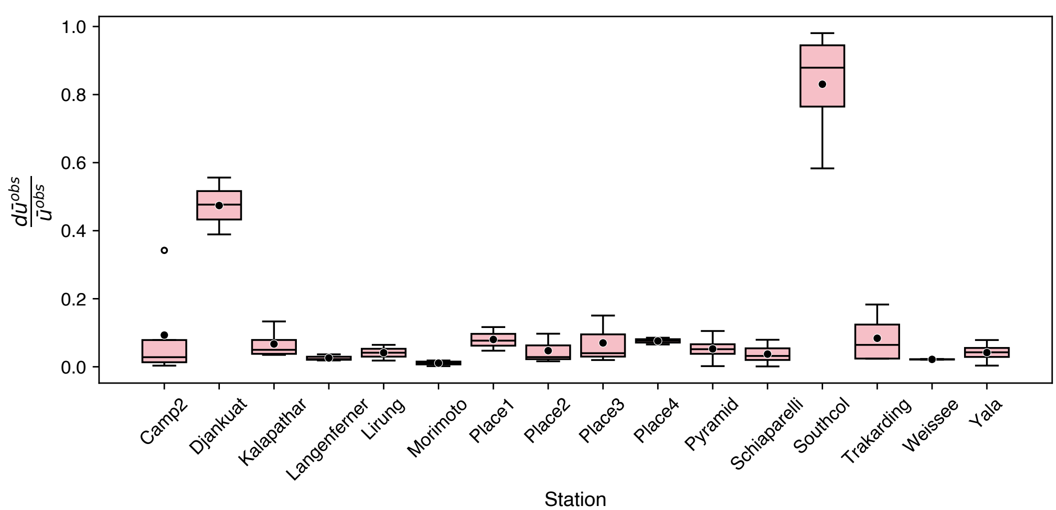

Figure S6. For the stations with more than one year of data, the box-plot shows the distribution of fractional absolute deviations $d\bar{u}/\bar{u}$ across different years. South Col station has the highest inter-annual mean wind speed variability. This is one among the three high-altitude stations (Balcony and Bishop are the other two) located near Mt. Everest, with possible influence of synoptic scale winds. Djankuat Glacier station, second among the two stations with the most inter-annual variability of mean wind speed, also has the highest observed mean wind speed among all stations. The winds in this station is predominantly katabatic. Djankuat is also the glacier with the largest inter-annual observed mean temperature variability.

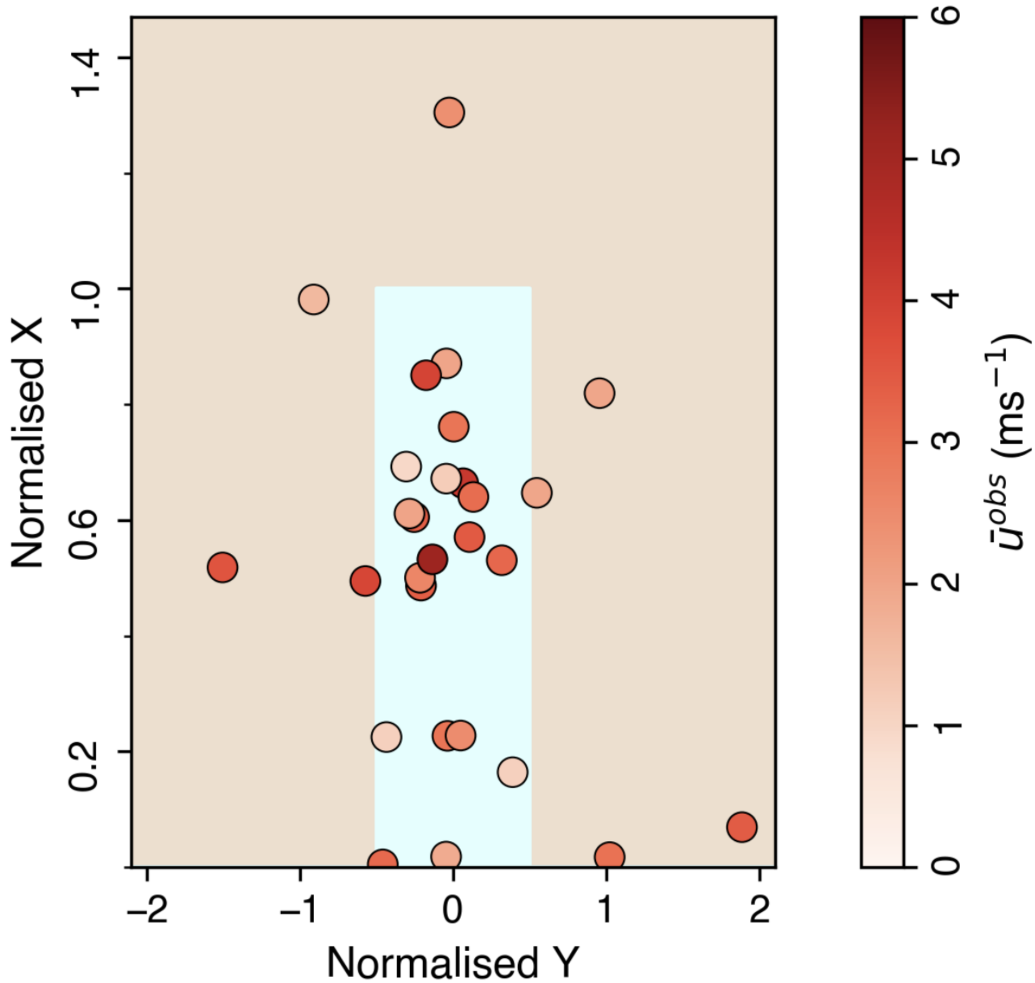

Figure S7. The observed mean wind speeds (shades of red) of 28 weather stations used in this study, with their relative locations (circles) shown on an idealised glacier (light blue rectangle) of unit length and width (similar to Figure 1b). No clear spatial pattern for winds could be seen from our dataset.

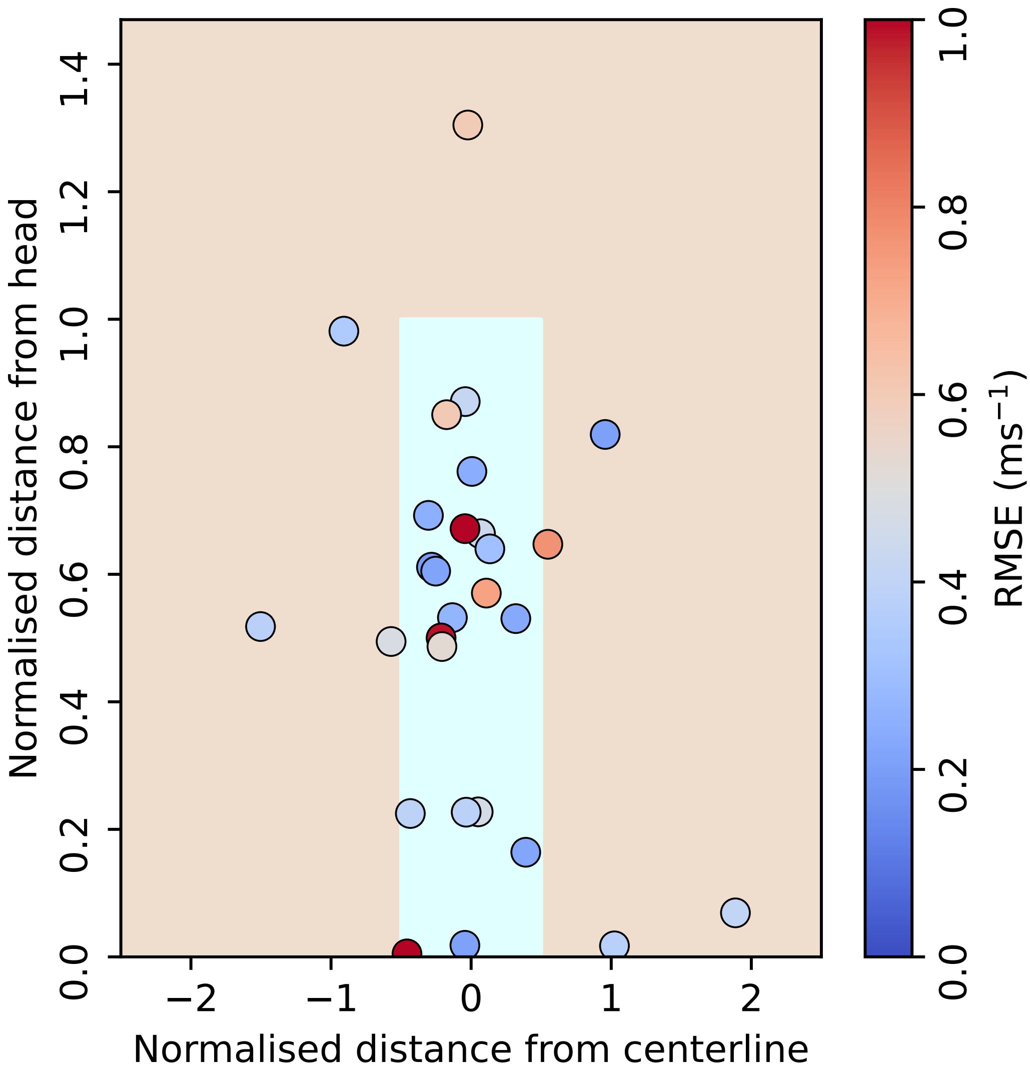

Figure S8. The RMSEs (shades of red and blue) in LOOCV analysis (main text, section 4.2.2) of 28 weather stations used in this study, with their relative locations (circles) shown on an idealised glacier (light blue rectangle) of unit length and width (similar to Figure 1b and S8). No clear spatial pattern for model performance could be seen from our dataset.

Table S1: Information about glaciers and the weather station datasets used in this work, and the associated glaciers

Station name, Data source	Station Type	Period for which data was available (number of summer days)	Latitude, Longitude	Elevation (m)	Glacier length (km)	Glacier area (km^2)	Mean temper-ature (°C)	Mean wind (m/s)	Glacier type
Arolla (Shaw, 2023)	On-glacier	2022-07-06 to 2022-09-18 (74 days)	45.97, 7.52	2852	4.4	3.8	7.4	3.4	Debris-free valley glacier
Balcony (Matthews and Coauthors, 2020)	Off-glacier	2019-06-01 to 2019-09-30 (122 days)	27.9826, 86.9292	8323	18.5	26.4	-16.7	3.4	Debris-covered valley glacier
Bellavista (Strasser and Marke, 2017)	Off-glacier	2015-07-27 to 2015-09-28 (64 days)	46.78284, 10.79138	2799	3.2	3.1	4.3	3.6	Debris-free valley glacier
Bishop (Matthews and Coauthors, 2020)	Off-glacier	2022-06-01 to 2022-07-29 (59 days)	27.9735, 86.9308	7857	18.5	26.4	-17.3	3.2	Debris-covered valley glacier
Camp2 (Matthews and Coauthors, 2020)	On-glacier	2019-06-01 to 2023-07-01 (518 days)	27.981, 86.9023	6485	18.5	26.4	-4.0	1.1	Debris-covered valley glacier
Chotta Shigri1 (Mandal et al., 2022)	On-glacier	2022-08-16 to 2022-09-29 (56 days)	32.2858, 77.5305	3844	9.5	16.8	0.0	2.4	Debris-free valley glacier
Chotta Shigri2 (Mandal et al., 2022)	On-glacier	2022-06-07 to 2022-09-29 (86 days)	32.228297, 77.506293	4871	9.5	16.8	2.4	2.6	Debris-free valley glacier
Djankuat (Rets and Popovnin, 2019)	On-glacier	2007-06-17 to 2009-09-30 (231 days)	43.198, 42.757	2976	3.2	3.0	7.0	5.1	Partly debris-covered-valley glacier
Drang Drung (This study)	On-glacier	2023-06-01 to 2023-09-23 (98 days)	33.787596, 76.333945	4601	24.7	68.4	5.5	4.2	Lake-terminating Debris-free valley glacier
Hinterisferner (Stocker-Waldhuber et al., 2013)	Off-glacier	2012-06-01 to 2012-09-30 (121 days)	46.79867, 10.76042	3027	8.5	8.0	4.3	3.9	Debris-free valley glacier
Kalapathar (EvK2CNR station)	Off-glacier	2009-06-01 to 2012-09-30 (457 days)	27.99, 86.83	5600	18.5	26.4	0.1	2.0	Debris-covered valley glacier
Kennikot (Buri et al., 2022)	On-glacier	2019-05-31 to 2019-08-21 (82 days)	61.4841, -142.9283	657	44.9	292.5	10.5	2.0	Debris-covered valley glacier
Langenferner (Galos, 2019)	Off-glacier	2013-06-01 to 2015-08-27 (332 days)	46.47245, 10.61391	2954	2.9	2.2	4.0	3.4	Debris-free valley glacier
Lirung (ICIMOD and Utrecht University, 2020a)	Off-glacier	2018-06-01 to 2019-08-10 (186 days)	28.24, 85.56	4276	8.6	4.8	8.1	1.0	Debris-covered valley glacier
Morimoto (ICIMOD and Utrecht University, 2020b)	Off-glacier	2017-06-01 to 2019-09-30 (365 days)	28.25296, 85.68152	4925	4.6	1.4	3.4	2.0	Debris-covered valley glacier
Place1 (Shea, 2010)	On-glacier	2006-08-04 to 2008-08-12 (206 days)	50.426073, -122.601628	1970	3.8	3.0	4.7	3.0	Debris-free valley glacier
Place2 (Shea, 2010)	On-glacier	2006-08-04 to 2008-09-28 (266 days)	50.421835, -122.598482	2025	3.8	3.0	4.5	3.1	Debris-free valley glacier
Place3 (Shea, 2010)	On-glacier	2006-08-04 to 2008-08-31 (241 days)	50.414718, -122.600217	2095	3.8	3.0	5.2	3.2	Debris-free valley glacier
Place4 (Shea, 2010)	On-glacier	2006-08-04 to 2008-08-25 (189 days)	50.412846 , -122.615898	2330	3.8	3.0	4.3	2.9	Debris-free valley glacier
Pyramid (EvK2CNR station)	Off-glacier	2009-06-01 to 2012-09-29 (473 days)	27.95792, 86.814807	5050	18.5	26.4	2.1	2.0	Debris-covered valley glacier
Satopanth (This study)	On-glacier	2017-06-29 to 2017-09-29 (92 days)	30.773251 , 79.408794	3910	20.1	57.0	9.7	1.2	Debris-covered valley glacier
Schiaparelli (Arigony-Neto et al., 2023)	On-glacier	2016-05-31 to 2020-09-09 (586 days)	-54.4, -70.87	197	10.8	24.8	7.1	3.9	Lake-terminating Debris-free glacier

Southcol (Matthews and Coauthors, 2020)	Off-glacier	2019-06-01 to 2023-07-04 (419 days)	27.9719, 86.9295	7905	18.5	26.4	-13.4	3.07	Debris-covered valley glacier
Trakarding (Fujita, Sunako, Sakai, 2021)	Off-glacier	2016-06-01 to 2019-09-29 (487 days)	27.843, 86.487	4821	17.9	32.1	4.6	1.6	Debris-covered valley glacier
Weart1 (Shea, 2010)	On-glacier	2007-07-10 to 2007-09-06 (58 days)	50.155944, -122.760257	2164	6.5	8.1	4.0	3.5	Debris-free valley glacier
Weart2 (Shea, 2010)	On-glacier	2007-07-10 to 2007-09-06 (58 days)	50.138823, -122.775232	2298	6.5	8.1	4.8	2.5	Debris-free valley glacier
Weissee (Stocker-Waldhuber et al., 2022)	Off-glacier	2017-06-01 to 2018-09-30 (243 days)	46.872909, 10.714437	3507	7.8	16.7	7.5	1.9	Debris-free valley glacier
Yala (ICIMOD, 2016)	Off-glacier	2016-06-01 to 2019-09-30 (464 days)	28.23, 85.62	5214	2.2	2.1	1.2	1.1	Debris-free cirque glacier

Table S2: Description of static variables used in section 3.1.2. Here, ALOS World 3d refers to the 30-m resolution digital elevation model from Tadono et al. (2014), GEE refers to Google Earth Engine (Gorelick et al., 2017), RGI7 refers to the Randolf Glacier Inventory 7 (RGI7.0-Consortium, 2023) and QGIS refers to the Geographic Information System (GIS) application (QGIS Development Team, 2024)

Symbol	Description	Unit	Source
L	Length of glacier	km	RGI7
$\bar{W}_g$	Mean width of glacier (A_g/L_g)	km	RGI 7
R_1	Difference between maximum and minimum elevation inside 1 km circular buffer of station	km	GEE and ALOS World 3D
Z_{range}	$Z_{max} - Z_{min}$	m	RGI7
R_5	Difference between maximum and minimum elevation inside 5 km circular buffer of station	km	GEE and ALOS World 3D
R_{10}	Difference between maximum and minimum elevation inside 10 km circular buffer of station	km	GEE and ALOS World 3D
σ_1	Standard deviation of elevations around 1 km square buffer of station	km	GEE and ALOS World 3D
σ_5	Standard deviation of elevations around 5 km circular buffer of station	km	GEE v ALOS World 3D
σ_{10}	Standard deviation of elevations around 10 km circular buffer of station	km	GEE and ALOS World 3D
$\varsigma_{0.1}$	Slope of DEM at the station, calculated from a 3x3 window of DEM cells after resampling to 100-m resolution	degrees	GEE and ALOS World 3D
ς_1	Slope of DEM at the station, calculated from a 3x3 window of DEM cells after resampling to 1-km resolution	degrees	GEE and ALOS World 3D
ς_{10}	Slope of DEM at the station, calculated from a 3x3 window of DEM cells after resampling to 10-km resolution	degrees	GEE and ALOS World 3D
ς^{rgi}	Slope of glacier	degrees	RGI7
$\bar{T}^{era}$	Mean summer months (JJAS) temperature of station derived	°C	ERA5L

Table S3: For each of the 28 stations, the RMSE between u^{pred} from the fitted model (Sect. 3.1.2), calibrated model (Section 3.2.1), and LOOCV model (Sect. 3.2.2) against u^{obs} is presented. The corresponding RMSEs for ERA5L winds are also included for comparison.

Station Name	Fitted Model	Calibrated Model	LOOCV Model	ERA5L
Arolla	0.26	0.48	0.49	0.49
Balcony	0.29	0.77	0.79	0.79

Bellavista	0.17	0.29	0.30	0.30
Bishop	0.36	0.89	0.91	0.91
Camp2	0.15	0.22	0.22	0.22
Chotta Shigri1	0.55	1.13	1.14	1.14
Chotta Shigri2	0.47	0.75	0.76	0.76
Djankuat	0.60	1.67	1.68	1.68
Drangdrung	0.25	3.00	3.02	3.02
Hinterisferner	0.12	0.82	0.85	0.85
Kalapathar	0.57	1.97	1.97	1.97
Kennikot	0.15	2.70	3.00	3.00
Langenferner	0.24	0.74	0.74	0.74
Lirung	0.11	0.79	0.80	0.80
Morimoto	0.38	0.81	0.81	0.81
Place1	0.04	0.40	0.40	0.40
Place2	0.05	0.46	0.47	0.47
Place3	0.04	0.47	0.48	0.48
Place4	0.12	0.42	0.42	0.42
Pyramid	0.54	1.25	1.26	1.26
Satopanth	0.36	0.87	0.87	0.87
Schiaparelli	0.05	0.25	0.25	0.25
Southcol	0.06	0.53	0.55	0.55
Trakarding	0.22	0.52	0.52	0.52
Weart1	0.07	0.39	0.39	0.39
Weart2	0.13	0.44	0.45	0.45
Weissee	0.17	0.32	0.33	0.33
Yala	0.14	0.42	0.43	0.43

Table S4: Comparison of the turbulent heat flux estimated using the simple bulk-aerodynamic model (Cuffey and Paterson, 2010). . The mean summertime air temperature T^{era} (°C), the dew-point temperature T^{era}_{dew} ((°C), and the surface pressure P (Pa) at each station are obtained from ERA5. The vapor pressure e (Pa) and saturation vapor pressure es (Pa) is calculated with P, Tera and Tdew by using the equation described in (Bolton, 1980; Buck, 1981). Using the methods described in section 2.6, we estimate sensible heat flux Q_{shf} (Wm^{-2}), latent heat flux Q_{lhf}(Wm^{-2}) and the total turbulent heat flux $Q_{thf} = Q_{shf} + Q_{lhf}$ (Wm^{-2}) for each station. The fluxes obtained when the mean wind speed is taken from our model ($\bar{u}^{pred}$), and those obtained directly from ERA5 ($\bar{u}^{era}$), are compared with the same estimated using mean wind speed observed at the station ($\bar{u}^{obs}$).

	Constants derived from ERA5L					**Mean wind speed**			**Sensible heat flux**			**Latent heat flux**			**Turbulent heat flux**		
Name	T^{era}	T^{era}_{dew}	e	e_s	P	$\bar{u}^{obs}$	$\bar{u}^{pred}$	$\bar{u}^{era}$	Q^{obs}_{shf}	Q^{pred}_{shf}	Q^{era}_{shf}	Q^{obs}_{lhf}	Q^{pred}_{lhf}	Q^{era}_{lhf}	Q^{obs}_{thf}	Q^{pred}_{thf}	Q^{era}_{thf}
Arolla	7.4	-0.1	606.2	1026.2	71993.5	3.4	3.7	0.8	46.2	50.5	11.6	-50.9	-55.6	-12.8	-4.6	-5.1	-1.2
Balcony	-8.7	-3.5	471.8	317.4	50300.3	3.4	2.8	0.8	-38.6	-31.3	-9.4	18.9	15.3	4.6	-19.7	-16.0	-4.8
Bellavista	4.1	0.9	650.4	816.6	72869.9	3.6	3.5	0.9	27.3	26.3	6.8	-21.3	-20.5	-5.3	6.0	5.8	1.5
Bishop	-6.5	-3.0	491.7	376.4	50665.5	3.2	2.4	0.7	-27.0	-20.3	-6.3	13.1	9.9	3.1	-13.9	-10.5	-3.3
Camp2	-1.3	-3.2	482.5	557.4	50563.6	1.1	1.1	0.8	-1.8	-1.7	-1.3	-3.0	-2.8	-2.1	-4.8	-4.6	-3.5
Chotta Shigri1	2.3	-0.4	593.4	718.6	58103.9	2.4	1.8	0.8	8.1	6.2	2.8	-10.8	-8.2	-3.7	-2.7	-2.0	-0.9
Chotta Shigri2	3.8	1.0	657.6	803.5	58176.7	2.6	3.1	0.8	15.0	17.5	4.5	-13.7	-15.9	-4.1	1.4	1.6	0.4
Djankuat	8.7	3.0	757.7	1125.0	71659.9	5.1	4.8	0.7	82.4	76.8	11.0	-67.3	-62.7	-8.9	15.1	14.1	2.0

Drang Drung	1.4	-4.3	445.3	675.2	56415.5	4.2	1.2	0.7	8.4	2.5	1.4	-34.6	-10.1	-5.8	-26.2	-7.6	-4.4
Hinterisferner	3.4	0.4	629.7	778.7	72919.5	3.9	3.2	0.8	24.7	20.1	5.1	-20.7	-16.8	-4.3	4.0	3.3	0.8
Kalapathar	0.3	-1.6	542.0	624.3	53165.7	2.0	0.5	0.9	0.8	0.2	0.4	-5.8	-1.5	-2.6	-5.0	-1.3	-2.2
Kennikot	10.7	7.1	1009.0	1287.0	90928.8	2.0	4.7	0.9	49.6	117.0	21.7	-19.6	-46.3	-8.6	29.9	70.7	13.1
Langenferner	6.5	2.5	730.3	970.7	75768.8	3.4	3.2	0.8	43.1	41.1	9.7	-29.0	-27.7	-6.6	14.1	13.5	3.2
Lirung	5.5	1.9	702.7	902.5	55918.3	1.0	1.7	0.8	7.6	13.6	6.6	-6.9	-12.2	-6.0	0.7	1.3	0.6
Morimoto	1.5	-0.3	598.0	680.6	53513.4	2.0	1.7	0.8	4.1	3.5	1.7	-5.9	-5.1	-2.5	-1.8	-1.5	-0.8
Place1	10.7	4.7	852.8	1286.9	87208.1	3.0	2.9	0.8	71.5	68.9	18.5	-46.1	-44.4	-11.9	25.4	24.5	6.6
Place2	10.5	5.1	876.2	1271.3	87209.5	3.1	2.8	0.7	73.3	67.1	17.7	-43.8	-40.1	-10.6	29.5	27.1	7.1
Place3	11.1	5.4	895.2	1320.8	87207.7	3.2	2.9	0.8	79.9	72.7	19.2	-48.8	-44.3	-11.7	31.2	28.4	7.5
Place4	11.1	5.3	889.8	1320.5	87216.8	3.0	2.9	0.8	73.8	72.7	19.0	-45.5	-44.9	-11.7	28.2	27.8	7.3
Pyramid	1.0	-3.6	469.2	659.1	50221.7	2.0	1.0	0.9	2.6	1.3	1.1	-13.3	-6.6	-5.8	-10.7	-5.3	-4.6
Satopanth	5.6	0.8	645.3	912.2	57746.3	1.2	1.8	0.8	10.0	15.1	6.7	-11.4	-17.2	-7.6	-1.4	-2.1	-0.9
Schiaparelli	7.0	3.5	783.5	998.9	96673.8	3.9	3.9	5.5	68.0	67.4	95.9	-30.2	-29.9	-42.6	37.8	37.5	53.3
Southcol	-7.2	-3.3	479.7	357.9	50518.7	3.0	2.5	0.8	-28.1	-23.4	-7.6	13.1	10.9	3.5	-14.9	-12.5	-4.0
Trakarding	5.4	2.3	718.8	896.6	55669.7	1.6	1.8	0.8	12.4	13.8	5.8	-10.2	-11.4	-4.8	2.2	2.5	1.0
Weart1	10.9	6.4	964.0	1301.7	85446.5	3.5	3.2	0.6	82.8	77.1	14.2	-41.7	-38.8	-7.1	41.1	38.2	7.0
Weart2	8.4	4.9	865.5	1101.4	82942.2	2.5	2.8	0.6	44.2	50.7	11.1	-20.8	-23.8	-5.2	23.4	26.8	5.9
Weissee	3.3	2.1	710.0	771.7	74833.8	1.9	2.1	0.7	11.7	13.2	4.7	-4.1	-4.7	-1.6	7.6	8.6	3.0
Yala	1.7	2.2	715.6	690.3	55965.1	1.1	1.5	0.8	2.7	3.5	2.0	1.0	1.3	0.7	3.7	4.9	2.7

References

Arigony-Neto, J., Jaña, R., Gonzalez, I., Schneider, C., and Temme, F.: Automatic Weather Station observations at Schiaparelli Glacier, Sep 2015 - Feb 2019, PANGAEA, https://doi.org/10.1594/PANGAEA.958693, in: Arigony-Neto, J et al. (2023): Meteorological Observations at Schiaparelli Glacier Automatic Weather Station (AWSglacier), Cordillera Darwin, Chile, 2013-2019 [dataset publication series]. PANGAEA, https://doi.org/10.1594/PANGAEA.958694, 2023.

Bolton, D.: The Computation of Equivalent Potential Temperature, Monthly Weather Review, 108, 1046 – 1053, https://doi.org/10.1175/1520-0493(1980)108<1046:TCOEPT>2.0.CO;2, 1980.

Buck, A. L.: New Equations for Computing Vapor Pressure and Enhancement Factor, Journal of Applied Meteorology and Climatology, 20, 1527 – 1532, https://doi.org/10.1175/1520-0450(1981)020<1527:NEFCVP>2.0.CO;2, 1981.

Buri, P., Truffer, M., Fochesatto, J., and Aschwanden, A.: Automatic weather station data from the debris- covered Kennicott Glacier, Alaska (May-Aug 2019), https://doi.org/10.5281/zenodo.6424158, 2022.

Cuffey, K. and Paterson, W.: The Physics of Glaciers, Academic Press, ISBN 9780080919126, https://books.google.co.in/books?id=Jca2v1u1EKEC, 2010.

Galos, S. P.: Weather Station raw-data Langenferner-Felsköpfl 2012-2015, https://doi.org/10.1594/PANGAEA.902771, 2019.

Gorelick, N., Hancher, M., Dixon, M., Ilyushchenko, S., Thau, D., and Moore, R.: Google Earth Engine: Planetary-scale geospatial analysis for everyone, Remote Sensing of Environment, https://doi.org/10.1016/j.rse.2017.06.031, 2017.

ICIMOD: Meteorological data from Yala Base Camp automatic weather station, [Data set], https://doi.org/10.26066/RDS.26859, accessed: 2025-07-22, 2016.

ICIMOD and Utrecht University: Micromet station: Lirung glacier, [Data set], https://doi.org/10.26066/RDS.1972409, accessed: 2025-07-22, 2020a.

ICIMOD and Utrecht University: Micromet station: Morimoto, [Data set], https://doi.org/10.26066/RDS.1972408, accessed: 2025-07-22, 2020b.

Mandal, A., Angchuk, T., Azam, M. F., Ramanathan, A., Wagnon, P., Soheb, M., and Singh, C.: An 11-year record of wintertime snow-surface energy balance and sublimation at 4863 m asl on the Chhota Shigri Glacier moraine (western Himalaya, India), The Cryosphere, 16, 3775–3799, 2022.

Matthews, T. and Coauthors: Going to Extremes: Installing the World's Highest Weather Stations on Mount Everest, Bulletin of the American Meteorological Society, 101, E1870–E1890, https://doi.org/10.1175/BAMS-D-19-0198.1, 2020.

QGIS Development Team: QGIS Geographic Information System, Open Source Geospatial Foundation Project, http://qgis.osgeo.org, 2024.

RGI7.0-Consortium: Randolph Glacier Inventory - A Dataset of Global Glacier Outlines, Version 7.0, https://doi.org/10.5067/f6jmovy5navz, 2023.

Shea, J. M.: Regional-scale distributed modelling of glacier meteorology and melt, southern Coast Mountains, Canada, Ph.D. thesis, University of British Columbia, https://doi.org/http://dx.doi.org/10.14288/1.0069481, 2010.

Stocker-Waldhuber, M., Emprechtinger, M., and Fischer, A.: Continuous meteorological observations at weather station HEF (Hintereisferner), Ötztal Alps, Austria, in 2012, https://doi.org/10.1594/PANGAEA.809095, 2013.

Stocker-Waldhuber, M., Seiser, B., and Fischer, A.: Meteorological data Weißseespitze/Austria, 2017-10-31 to 2018-09-30, PANGAEA, https://doi.org/10.1594/PANGAEA.939824, 2022.

Strasser, U. and Marke, T.: Continuous meteorological observations at station Bella Vista in 2016, PANGAEA, https://doi.org/10.1594/PANGAEA.879211, 2017.

Tadono, T., Ishida, H., Oda, F., Naito, S., Minakawa, K., and Iwamoto, H.: Precise Global DEM Generation by ALOS PRISM, ISPRS Annals of the Photogrammetry, Remote Sensing and Spatial Information Sciences, II-4, 71–76, https://doi.org/10.5194/isprsannals-II-4-71-2014, 2014.